Experimental Investigation of Loading Effects on Compressor Trailing-Edge Flowfields

Duane C. McCormick* and Robert W. Paterson†
United Technologies Research Center, East Hartford, Connecticut 06108
and
Harris D. Weingold‡
Pratt & Whitney, Commercial Engine Business, East Hartford, Connecticut 06108

This article describes an experimental investigation of the flowfield development in the trailing-edge region of a simulated compressor airfoil having pressure-to-suction surface loading. The study represents a continuation of an effort to study turbulent, separated airfoil trailing-edge flows. Previous experimentation had addressed airfoil trailing-edge separation phenomena in the absence of pressure loading. The objective of the current study was to explore the effects of loading and thereby to provide a more realistic simulation of the compressor airfoil flow environment. The present approach was to conduct a large-scale cascade simulation of the airfoil trailing-edge flowfield for both a nominal design condition and a higher loading off-design condition. For the design condition, the airfoil boundary layers separated on the blunt trailing edge. For the off-design condition, separation occurred on the suction surface upstream of the trailing edge. A principal result of the study was that pressure loading was found to alter the trailing-edge time mean velocity field from that observed in the previous unloaded airfoil experiment. The relative base pressure for the nominal design condition was unaltered from the unloaded experiment but significantly lower for the off-design condition. Increased loading was found to induce greater cascade exit flow deviation from the exit metal angle, thus, reducing the relative cascade flow turning.

Nomenclature

C_p = pressure coefficient, $(P - P_{ref})/Q_{ref}$
C_{pte} = pressure coefficient for trailing-edge region, $(P - P_{ex})/Q_{ex}$
H = shape factor
P = static pressure
P_t = reference, cascade-inlet total pressure
Q = dynamic head, $(P_t - P)$
s = surface coordinate measured from trailing edge
t = trailing-edge thickness
x = coordinate parallel to exit camber line
y = coordinate normal to exit camber line
y_{bl} = boundary-layer coordinate normal to surface
δ^* = displacement thickness
θ = momentum thickness
ψ = stream function

Subscripts

ref = reference, cascade-inlet condition
ex = cascade-exit condition

Introduction

THE overall research problem addressed in this study was turbulent boundary layer separation in the trailing-edge region of compressor airfoils. Because of the thick, blunt trailing-edge geometries for structural and durability reasons, surface curvature-induced separation invariably occurs in this region at design conditions. Under higher loading conditions associated with off-design operation, the suction surface separation location moves forward, resulting in a larger spatial extent of the separated flow region.

One undesirable consequence of trailing-edge separation is failure to recover total pressure at a rearward stagnation point. Hence, separation results in a depressed base pressure and a drag contribution, which can be an appreciable portion of the overall drag for an otherwise well-designed airfoil. A second undesirable consequence is that separation decreases flow turning, thereby, reducing airfoil lift. In more extreme loading situations, the suction surface separation can move forward from the trailing edge, resulting in stall and catastrophic loss of lift.

The cascade study of Hobbs et al.[1] and the unloaded blunt-based airfoil study of Paterson and Weingold[2] are examples of previous experimental programs directed toward improving understanding of the compressor airfoil trailing-edge separation phenomenon. The compressor cascade study of Hobbs et al.[1] provided information on overall trailing-edge flow characteristics. Because of the small scale of the experiment, the detailed definition of the separated flow region required for code assessment and development efforts was not provided. This lack of resolution led to a previously reported experiment[2] in which a large-scale airfoil model was used to provide detailed information regarding trailing-edge pressure distributions, velocity fields, and unsteady flow (vortex shedding) characteristics. The focus of that study was a test condition where the effect of turbulent boundary layer to trailing-edge thickness ratio could be explored without the presence of pressure loading effects. The test conditions were near equilibrium boundary layers in the one to two trailing-edge thickness range, typical of supercritical compressor airfoils, with a zero pressure gradient freestream boundary condition. The study produced the desired detailed flowfield information and identified vortex shedding as an important flow feature. It was further found that unsymmetric boundary layers with a relative thickness ratio of 1.8 (in displacement, momentum, and boundary-layer thickness), but similar shape factors, had a negligible influence on the flowfield.

Presented as Paper 88-0365 at the AIAA 26th Aerospace Sciences Meeting, Reno, NV, Jan. 11-14, 1988; received Nov. 14, 1988; revision received Nov. 5, 1989.

*Research Engineer. Member AIAA.
†Manager Gas Dynamics and Thermophysics. Associate Fellow AIAA.
‡Senior Research Scientist. Associate Fellow AIAA.

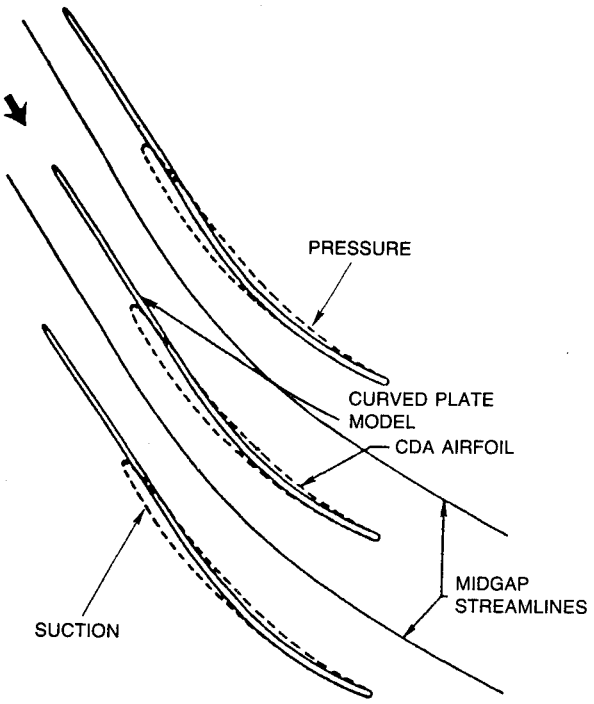

Fig. 1 Schematic of curved-plate cascade simulation.

The overall goal of the present effort was to extend the previous research to include realistic trailing-edge loading conditions, thereby including the remaining major effect expected to influence separation characteristics. The approach was to conduct a large-scale cascade simulation using contoured wind tunnel walls to simulate midgap streamlines. The pressure distribution was designed to simulate that which would be obtained in a controlled diffusion airfoil (CDA) cascade. CDA refers to a supercritical compressor airfoil design described by Hobbs and Weingold.[3] Two compressor operating conditions were investigated. The first, termed the low loading case, addressed on-design operation where separation occurs on the trailing-edge circle. The second, high loading case was concerned with off-design operation, where the separation region expands to include a portion of the suction surface just upstream of the trailing edge.

Experimental Description

Approach

As in the previous study,[2] a large-scale plate of constant thickness was used to simulate the compressor airfoil. The scale of the experiment (trailing-edge diameter of 2.54 cm) was set by the need to acquire a detailed definition of the velocity and pressure fields in the vicinity of the trailing edge. The length of the plate was selected to provide ratios of turbulent boundary-layer thickness to trailing-edge thickness representative of actual scale applications. Typical boundary-layer characteristics for supercritical airfoils are given by the Build I cascade data reported by Hobbs et al.[1] At a position 0.03 chord upstream of the trailing edge, ratios of pressure surface and suction surface momentum thickness to trailing-edge diameter were 0.09 and 0.26, respectively. To achieve relative thickness in this range, a plate length on the order of 2 m was required. A curved plate contained within a contoured wind tunnel duct was used to generate pressure gradient histories typical of a CDA cascade. The contoured wind tunnel walls represent the midgap streamlines corrected for boundary-layer growth. Relative to flow conditions, the approach was to conduct the experiment at a low subsonic Mach number in a two-dimensional flow environment. Modeling of compressibility effects was not considered to be of first order importance.

The pressure distribution of the CDA cascade B, one of eight CDA cascades described by Hobbs and Weingold,[3] was selected for use in the present study. This design is typical of that employed in the rotor tip region of a compressor middle stage. Translation of this design into a wind tunnel configuration is given by McCormick et al.[4,5] Figure 1 shows the relationship of the original airfoil and cascade arrangement (dashed lines) to the curved-plate simulation.

Wind Tunnel Arrangement

The experiment was conducted in the United Technologies Research Center (UTRC) Boundary-Layer Wind Tunnel with a cascade simulation test section. The wind tunnel is a low-speed, closed-looped, low turbulence (0.25%) design. A side-view schematic diagram of the facility with the cascade simulation test section is shown in Fig. 2.

The wind tunnel blower is located upstream of the settling chamber. Perforated plates, honeycomb, and screens are used in the chamber to provide uniform, low turbulence flow. Downstream of the flow conditioning, the flow is accelerated through a 2:1 contraction. The initial portion of the test section is a straight duct with cross-sectional dimensions of 79-cm span and 42-cm height. The upstream, flat plate portion of the model is mounted in this duct (see Fig. 3). The straight duct is followed by flexible polypropylene walls, which represent the displaced (boundary layer corrected) midgap streamlines. The midgap streamlines terminate at the downstream dump region. The flow is then ducted into the submicron filter system and heat exchanger section of the return loop.

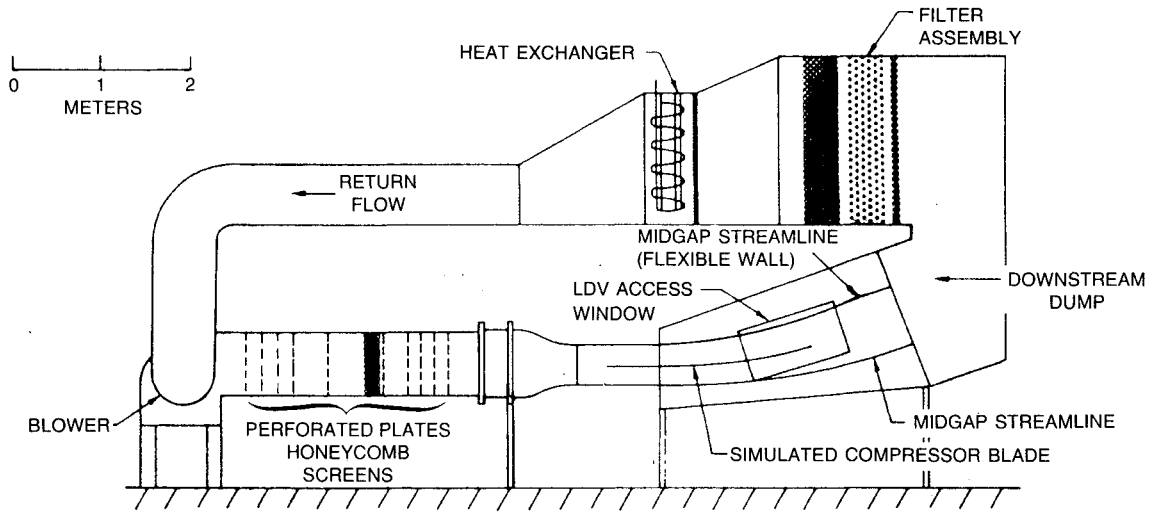

Fig. 2 Wind-tunnel arrangement.

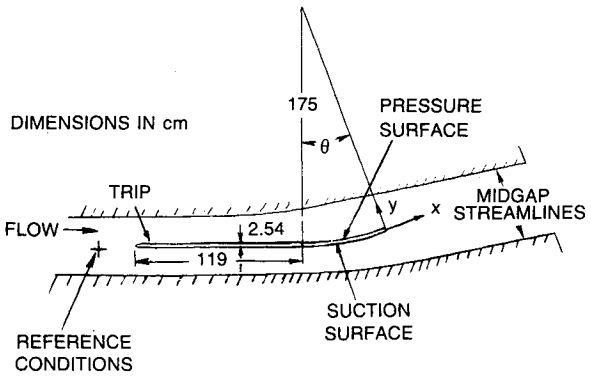

Fig. 3 Cascade simulation geometry.

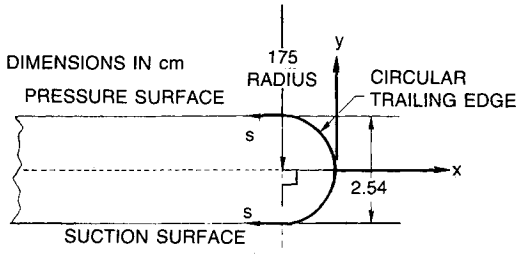

Fig. 4 Detail of trailing-edge geometry.

For the high loading case, the large transverse pressure gradient (caused by turning) interacted strongly with the corner boundary layers, giving rise to corner vortex structures that deteriorated the two dimensionality of the wind tunnel. This problem is typical of cascade facilities and is usually solved by corner bleed on the suction surface.[6] The same method was used here to correct the problem.

Airfoil Description

The model consists of two basic sections, the upstream flat plate section and the downstream turning section as shown in Fig. 3. Both sections are of aluminum rib construction with aluminum skin. The thickness is constant at 2.54 cm. The leading edge shape of the flat plate section is a 4 to 1 ellipse. The distance from the leading edge to the end of the flat plate section is 119 cm for both loading cases. The turning or loading section of the model is a circular arc of 175 cm mean radius. The low loading case has a 20-deg arc and the high loading case has a 30-deg arc. The shape of the trailing edge is a half circle of radius 1.27 cm and is tangent to the end of the turning section as shown in Fig. 4. To avoid three-dimensional transition, the model boundary layers were tripped on the flat plate section, 15.2 cm downstream of the leading edge. The trip was 0.38 mm thick and of the Hama type.[7] This thickness was designed to be 80% of the estimated displacement thickness to provide an efficient trip. The model coordinate system (x,y) has its origin located at the trailing edge with the x axis parallel to the exit mean camber line as shown in Fig. 4. The surface coordinate s is measured from the trailing-edge centerline and is used to report the surface pressure data.

Reference Conditions

The experiment was performed at constant Reynolds numbers of 2.6×10^6 and 3.0×10^6 for the low and high loading cases, respectively. This Reynolds number is based on the inlet velocity and the airfoil chord. The inlet or reference conditions of the wind tunnel were monitored upstream (9 model thicknesses) of the leading edge in the straight duct as shown in Fig. 3. The inlet velocity was nominally 24.0 m/s.

For the most part, the conditions measured at this location are used as the reference quantities for normalizing data acquired in the trailing-edge vicinity. The inlet velocity is designated U_{ref} and is used to normalize the velocities for the hot film and laser Doppler velocimetry (LDV) surveys. The inlet pressures are designated P_{ref} (reference static) and Q_{ref} (reference dynamic head) and are used (except where noted) to compute the surface pressure coefficients.

Instrumentation

The LDV equipment was a Thermal Systems Inc. (TSI) 9100-7, four beam, two color system (two velocity components). A counter-type processor was used to analyze the Doppler signal. The seed material was 1.07 μm polymer microspheres with a specific gravity of 1.05. The seed was mixed with alcohol and injected upstream of the wind tunnel contraction with a Wright jet baffle atomizer. The alcohol, after injection into the stream, would quickly evaporate leaving only the seed material. The worst case uncertainty (random and bias) in the mean velocity value was calculated to be $\pm2\%$ of the reference (cascade inlet) velocity.[4]

The hot film anemometry equipment was a TSI model 1050 general purpose unit operated in the constant temperature mode. The probe diameter and length was 0.05 and 1 mm, respectively, which was run at an overheat ratio of 1.5. The uncertainty in the hot film was estimated to be $\pm3.5\%$ of the reference velocity.[4]

Surface static pressures were measured with a Pressure Systems Inc. (PSI) model 780B/T pressure scanner. The uncertainty in the pressure coefficients was calculated to be $\delta C_p = \pm0.008$ and $\delta C_{pte} = \pm0.020$.[4]

Results

Static Pressure Distributions

Surface pressure distributions for the low and high loading cases are shown in Fig. 5 in terms of the pressure coefficient. The pressure coefficient C_p is based on the reference (inlet) conditions and is plotted vs the surface coordinate s/t measured from the trailing edge. The open symbols are for the low loading case, and the closed are for the high loading case. For reference purposes, sketches of the low and high loading model geometries are given below the figure. Note the overall length of the high loading case is longer due to the larger turning arc.

As is evident by the area between the suction and pressure surface distributions, the lift is larger for the high loading case. The main difference between the low and high loading cases (besides the overall loading) is the way in which the suction surface distribution approaches the trailing edge. For the high loading, the pressure distribution becomes flat over the last 4-5 trailing-edge thicknesses. This constant pressure is indicative of boundary-layer separation. Flow visualization also con-

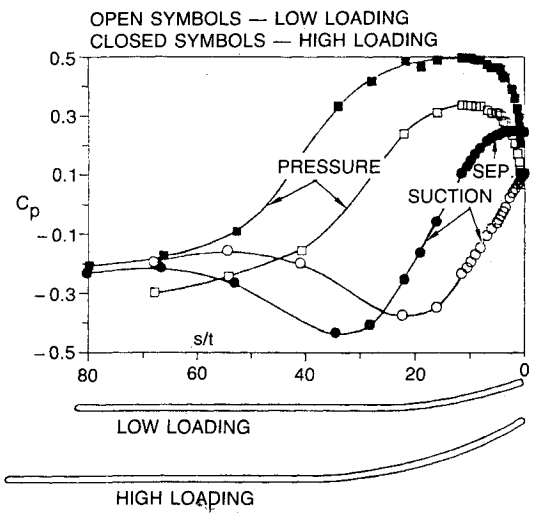

Fig. 5 Overall surface pressure distributions.

firmed this observation (and the location is shown in the figure). Thus the adverse pressure gradient on the suction surface is sufficient to separate the boundary layer.

In order to compare the trailing-edge pressure distributions among the two loading cases and the unloaded case of Paterson and Weingold,[2] it is necessary to scale the surface pressures in a different manner. Cascade-exit static pressure is a suitable pressure reference for the current study and can be considered to correspond to the constant freestream static pressure reference used in the previous unloaded study. Using cascade-exit static pressure as a reference, the trailing-edge pressure coefficient C_{pte} is defined as and related to C_p by

$$C_{pte} = \frac{(P - P_{ex})}{Q_{ex}} = 1 + \frac{Q_{ref}}{Q_{ex}}(C_p - 1)$$

The dynamic head ratio Q_{ref}/Q_{ex} is 1.333 and 1.754 for the low and high loading cases, respectively.

Surface pressure data over the last eight thicknesses are shown in Fig. 6a and the last two thicknesses in Fig. 6b in terms of the above described trailing-edge scaling. In addition to the two loading cases of the current experiment, the unloaded case of Paterson and Weingold[2] is also shown. As indicated, the trailing-edge surface extends over the region $s/t < \pi/4$. Also, pressure and suction surface separation locations are indicated by arrows labeled "Press. Sep." and "Suct. Sep.," respectively, as determined by surface flow visualization.

Low Loading

For the low loading case, the pressure surface distribution (open squares) over the last $8t$ is characterized by decreasing pressure from a value above the cascade-exit pressure to a local minimum on the trailing-edge circle. On the trailing-edge circle, the pressure quickly rises (with a slight overshoot) to the base pressure value (-0.2). The angular location on the trailing-edge circle of the local minimum pressure is approximately 8.5 deg measured from the pressure surface/trailing-edge circle interface. Flow visualization indicated boundary-layer separation occurred at a 17-deg location (as shown in the figures). Based on these observations, the local minimum is due to the

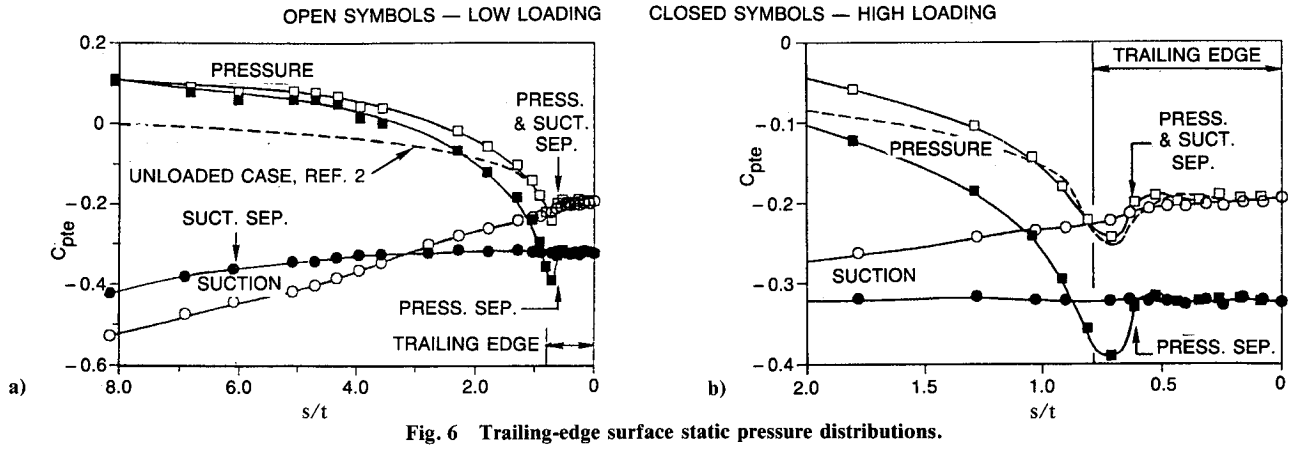

Fig. 6 Trailing-edge surface static pressure distributions.

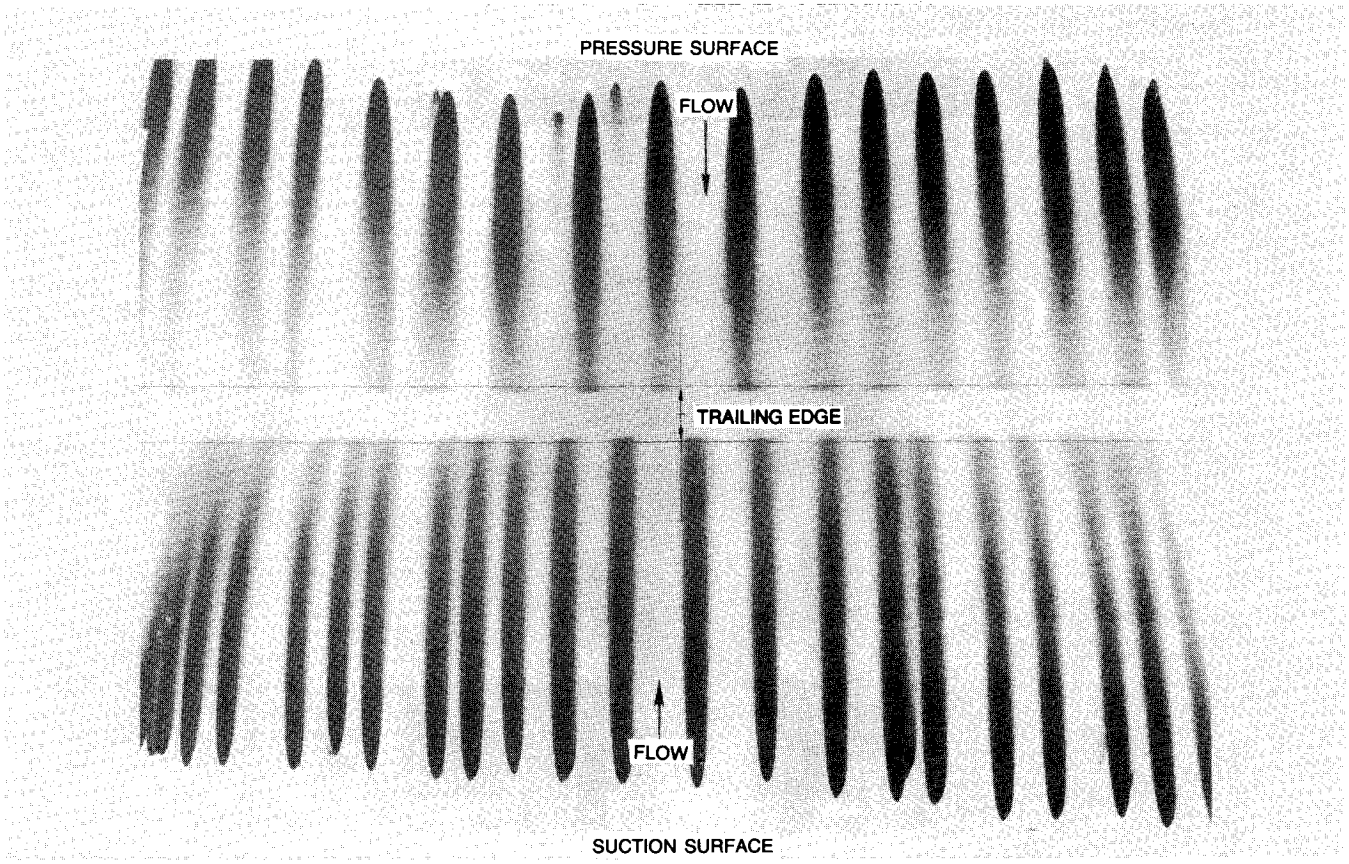

Fig. 7 Surface flow visualization, low loading.

local turning (expansion) on the trailing-edge circle. When the pressure begins to rise (to match the trailing-edge pressure), the adverse gradient quickly separates the boundary layer.

The suction surface pressure distribution is characterized by a relatively slow, monotonic pressure rise to the trailing-edge value. Flow visualization indicated the suction surface boundary layer separated at an angular location of 18 deg on the trailing-edge circle. Since the distribution displays no appreciable changes in the vicinity of 18 deg, it appears that no significant local turning has occurred.

High Loading

The high loading case is characterized by several notable differences relative to the low loading case. Most obvious is the lower base pressure value (-0.32). The suction surface distribution (solid circles) is nearly flat over the last 5 trailing-edge thicknesses due to the separation upstream of the trailing edge having a value equal to the base pressure value. The pressure surface distribution (solid squares), upstream of $6t$, is the same as the low loading case. Near the trailing edge, the pressure begins to drop more rapidly to the lower base pressure value.

If this trailing-edge scaling is relevant, then presumably different loading cases for which the suction boundary layer remains attached up the trailing edge would collapse to the current low loading case distribution. Thus, it is speculated that the lower base pressure value for the high loading case is due to loss in pressure recovery on the suction surface from the premature boundary layer separation. A simplified view of this complex interaction process is that the amount of suction surface pressure recovery determines the base pressure value and the pressure surface flow accelerates to this value.

Unloaded Case

The unloaded case studied by Paterson and Weingold[2] is compared with the current data in Figs. 6. Their experimental model was a flat plate terminated with the same trailing-edge geometry. Wind tunnel speeds and scales (trailing-edge size and boundary-layer thicknesses) were similar to the current experiment. The boundary conditions on the model were constant freestream velocity upstream and downstream of the trailing edge. Thus this experiment isolated the effects of the trailing edge from overall turning effects.

The unloaded case is shown as the dashed line in the figures. Since this case was symmetrical, the dashed line represents both the upper and lower surfaces. As shown in Fig. 6a, the pressure at $s/t = 8$ is the (constant) freestream value. Downstream of this point the effects of the trailing edge begin to lower the pressure below this value. That is, the local inviscid flow begins to accelerate. Over the last trailing-edge thickness

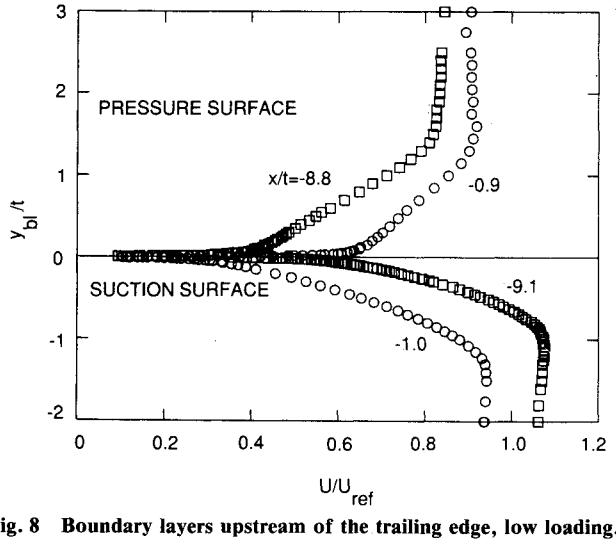

Fig. 8 Boundary layers upstream of the trailing edge, low loading.

Table 1 Upstream boundary-layer characteristics

Low loading							
Pressure surface				Suction surface			
x/t	δ^*/t	θ/t	H	x/t	δ^*/t	θ/t	H
−8.75	0.676	0.394	1.67	−9.10	0.108	0.068	1.58
−0.90	0.216	0.166	1.31	−1.00	0.344	0.194	1.77
High loading							
Pressure surface				Suction surface			
x/t	δ^*/t	θ/t	H	x/t	δ^*/t	θ/t	H
−8.15	0.493	0.330	1.50	−9.40	0.443	0.225	1.97
−1.00	0.253	0.204	1.24	−4.85	0.813	0.296	2.75
—	—	—	—	−0.75	1.200	0.327	3.24

($s/t < 1.25$), the distribution is remarkably similar to the low loading pressure surface distribution (see Fig. 6b). The base pressure values for the unloaded and low loading cases are identical.

In the unloaded flat plate study and cylinder studies (for example, see Roshko[8]), it has been shown that suppression of vortex shedding by insertion of a wake splitter plate raises base pressure significantly. Thus, trailing-edge separation contributes to low base pressure first by preventing recovery of pressure at a rear stagnation point and second by producing free shear layers, which roll-up into a vortex street. The good agreement between low loading and unloaded case base pressures suggests (and is indeed the case) separation locations and vortex shedding characteristics are similar. The further depression in base pressure for the high loading configuration appears to be due to failure of the suction surface flow to turn toward the trailing-edge centerline and to recover pressure due to upstream separation.

Flow Visualization

Flow visualization was used to define the two dimensionality of the flow and the location of separation lines. The main technique used in this experiment was an ammonia/reactor method for surface flow visualization. An example result is shown in Fig. 7, which is an "unwrapped" view of the pressure, trail-edge, and suction surfaces. Dark streaks represent attached flow. The flow on the pressure surface is observed to be two dimensional over nearly the entire span of the model. On the suction surface, there is a noticeable migration of the flow towards the center of the span due to corner boundary-layer interaction with the cascade pressure gradients. Such migration is typical of experimental cascades where corner suction is usually applied to reduce the interaction.[6] For this case, no corner suction was applied since the flow was two dimensional over 65% of the span. For both surfaces, the flow was found to separate on the trailing-edge circle at approximately an 18-deg angular location (measured from the pressure or suction surface/trailing-edge interface). It is presumed that separation points are unsteady due to the vortex shedding and lack of a salient edge. The pressure surface separation line was noticeably more defined than the suction surface (i.e., the pressure surface trace ended more abruptly). Therefore, the suction surface separation line appears to be more unsteady relative to the pressure surface separation.

The flow on the pressure surface for the high loading case was observed to be two dimensional over nearly the entire span. The separation was very similar to the low loading case. The flow appeared to negotiate the trailing-edge circle slightly further to a 19–20-deg angular location. For the suction surface, it was necessary to apply corner suction to achieve two-dimensional flow. The flow was observed to separate 5–6 trailing-edge thicknesses upstream of the trailing edge. The separation line, however, was not clearly defined and thus intermittent in nature. Smoke flow visualization with stroboscopic photograph confirmed this intermittent behavior. The strobe frequency was varied close to the fundamental shedding

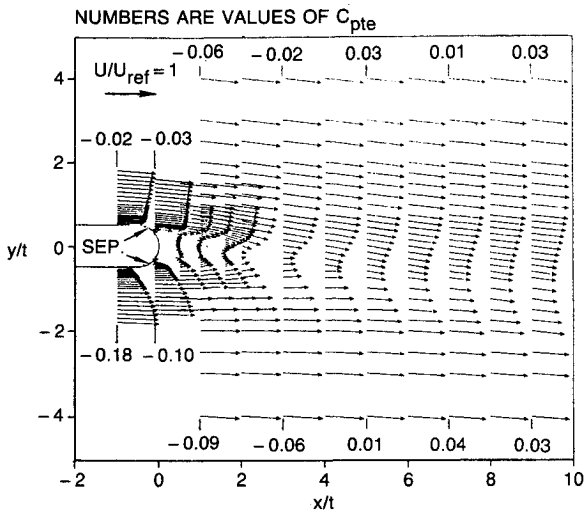

Fig. 9 Overall velocity vectors, low loading.

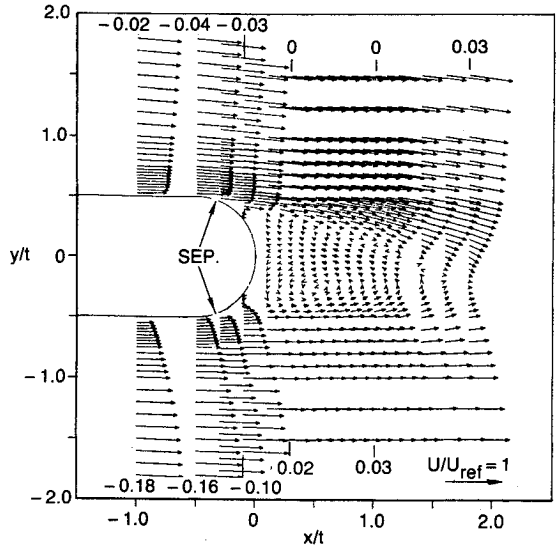

Fig. 10 Near wake velocity vectors, low loading.

frequency in an attempt to beat with any periodic motions. Since no periodic structure was observed, it is concluded that the intermittent separation is random in nature and not driven by the vortex shedding.

Intermittent suction surface separation has been observed in a double circular arc airfoil cascade.[9] Intermittent separation of the turbulent boundary layers on flat plate test surfaces caused by imposed adverse pressure gradients has also been studied by Patrick,[10] among others. Such intermittency appears to be a characteristic of separation from surfaces having low surface curvature. On the trailing-edge circle, the high curvature fosters separation at an approximately fixed location.

Boundary Layers Upstream of Trailing Edge

The boundary layers approaching the trailing edge on the suction and pressure surface were defined in detail with hot film anemometry. Boundary-layer characteristics were measured 8–9 trailing-edge thicknesses upstream of the trailing edge where surface static pressures indicated trailing-edge effects were small. Also, profiles were defined just upstream of the trailing edge to provide information on boundary-layer development under the influence of the freestream pressure gradients and to define the boundary-layer characteristics just upstream of the trailing edge. The characteristics of boundary layers just upstream of the trailing edge were found to have a strong effect on the flow downstream of the trailing edge.

Table 1 gives a listing of the boundary-layer characteristics in terms of displacement and momentum thickness and shape factor (note the approximate surface coordinate s/t can be found by adding 0.29 to the absolute value of x/t).

Figure 8 shows the boundary layers upstream of the trailing edge for the low loading case. The pressure surface boundary layer is nominally $1.8t$ thick over the last 10 trailing-edge thicknesses. The upstream profile has a relatively large shape factor (1.7) due to the adverse pressure gradient history (see Fig. 5, $s/t > 10$). From the upstream survey location to the trailing edge, the flow accelerates to meet the trailing-edge condition. In response to the favorable pressure gradient, the shape factor decreases to 1.3, indicating a healthier boundary layer. The boundary layer on the suction surface over the last 10 trailing-edge thicknesses was somewhat thinner in boundary-layer thickness at $1.3t$–$1.5t$. Note that both surveys are in the decelerating (adverse pressure gradient) portion of the suction surface (Fig. 5, $s/t < 10$). Over this region the shape factor increases from a relatively high value of 1.6 to a higher value of 1.8, indicative of a boundary layer approaching separation. In terms of the ratio of momentum thickness to trailing-edge thickness, the pressure and suction surface values at $x/t = -1$ were 0.166 and 0.194, respectively. These values are close to the unloaded case[2] values (0.1–0.17) and within the Build I (CDA) cascade range[1] (0.09–0.26).

The high loading profiles on the pressure surface were qualitatively very similar to the low loading profiles, but somewhat thicker at $2.3t$. As seen in the table, the pressure surface data are consistent with the low loading results. For the suction surface boundary layers, an intermediate profile was taken at $x/t = -4.9$ to detail the rapid growth of the boundary layer. The corresponding pressure gradient, shown in Fig. 5 ($s/t < 10$), displays decelerating flow followed by a constant pressure region indicative of boundary-layer separation. The growth of the boundary-layer thickness over the last nine trailing-edge thicknesses is from approximately $1.5t$ to $2.7t$. This growth rate is five times the rate for the low loading case. The shape factor starts at a very high value of 2.0 and increases to 3.2, indicative of boundary-layer separation. This behavior is consistent with flow visualization, which showed that an unsteady (intermittent) flow separation existed over the last 5–6 trailing-edge thicknesses.

In summary, hot film measurements taken upstream of the trailing edge showed boundary-layer characteristics consistent with the imposed pressure gradient histories. Momentum thickness to trailing-edge thickness ratios were in the range typical of CDA cascades used in full scale applications.

Vortex Shedding

Vortex shedding from the model trailing edge was present for both the low and high loading cases as indicated by hot film autospectral density functions taken in the wake. Results are generally similar to the previous unloaded experiment (flat plate with the same trailing-edge geometry) of Paterson and Weingold.[2] Unlike their results, however, histograms of the transverse velocity component in the current experiment did not show double peaked characteristics.[4]

For both loading cases, the spectral distributions indicated a discrete frequency in the wake corresponding to the fundamental shedding frequency. The low loading frequency was 130 Hz, whereas the high loading frequency was 60 Hz. At the wake edge, where the broadband random signal is small, it is evident that the "discrete" frequency is quite wide and is thus actually a narrow-band random signal. This suggests the shedding frequency modulates, presumably due to random variations of the inlet boundary layers.

To correlate the shedding frequencies of the different cases, the Strouhal number $St = f\ell/U$ was calculated. Here, f is the vortex shedding frequency, ℓ is the characteristic length, and U is the average freestream velocity in the trailing-edge region.

Using the trailing-edge thickness as the characteristic length gives values of 0.16 and 0.08 for the low and high loading cases, respectively. However, using a characteristic length based on the trailing-edge thickness plus the boundary-layer displacement thicknesses (pressure and suction), calculated just upstream of the trailing edge, yields Strouhal numbers of 0.23 and 0.19. These values are more typical of bluff body shedding. For the unloaded case, the Strouhal number (with displacement thicknesses added) was 0.22, which is in good agreement with the current results.

Flowfield Downstream of Trailing Edge

Vector representation of the LDV velocity data is shown in Fig. 9 for the low loading case. A detail of the near trailing-edge region is shown in Fig. 10. Separation locations on the model, derived from surface flow visualization, are indicated in the figures. Each vector represents the estimated time mean magnitude and flow direction of the velocity. The unit length of the vector relative to the reference velocity (U_{ref}, inlet velocity) is shown in the figures. The numbers in the figures indicate the freestream pressure coefficients C_{pte} estimated by the velocity data at the edges of the surveys. For this scaling a value of zero corresponds to a value equal to the cascade-exit velocity.

As illustrated in the overall view, Fig. 9, the boundary layers and freestream flow approaching the trailing edge are clearly attached and in the general direction of the surface. The pressure surface boundary layer is observed to be more full and healthier than that of the suction surface due to the opposite pressure gradient histories upstream of the trailing edge. The differences in the velocity profiles are quantified by the shape factors described earlier. The hot films surveys just upstream of the trailing edge give shape factor values of 1.77 for the suction surface and 1.31 for the pressure surface. This difference in velocity profiles (shape factor) causes a corresponding larger velocity gradient through the shear layer on the pressure side of the wake.

As observed in Fig. 9, the entire flowfield (excluding the immediate wake region) shows a general downward velocity component. Outside the wake, the flow angle on the pressure side is nearly constant at 6 deg from the trailing-edge metal angle. For the suction side, the flow angle is nearly constant at 4 deg from the metal angle. It is not evident what amount of the flow deviation is due to viscous effects since the kutta condition for a blunt-based airfoil is not well defined.

Downstream of the trailing edge, the flow from both sides generally turns inwards, filling in the wake behind the trailing edge. From Fig. 10 it is clear that the flow from the pressure surface turns more into the wake than the suction surface flow. This greater turning is most likely due to the larger velocity gradient on the pressure side shear layer. The probable mechanism is increased fluid entrainment by the pressure side shear layer, which locally reduces the static pressure on the low velocity side of the shear layer and induces it to turn more into the wake. This increased pressure side turning induces the outer flow on the pressure side to deviate further from the metal angle (6 deg compared to 4 deg for the suction side).

Note that a significant normal pressure gradient does not exist in the immediate inviscid region downstream of the trailing edge, as shown in Fig. 10 by the freestream pressure coefficient values. Based on these observations, it is concluded that the inviscid normal pressure gradient does not play a role in the increased pressure side turning into the wake.

In the wake downstream of the trailing edge, a separation bubble with two recirculation regions is present (at least in the time mean sense) as shown in the detailed vector plot of Fig. 10. The axial extent of the separation bubble is about $1.5t$. The two recirculations appear to be asymmetric. This asymmetry is brought out in the streamline analysis discussed subsequently. The unloaded case[2] indicated a time mean separation bubble with two symmetric recirculations; however, the bubble was shorter in the axial extent, closure occurring at $0.8t$. Also note in the figure, the first surveys downstream of the separation points do not show reversed flow since the separation is very thin relative to the LDV spatial resolution.

Corresponding presentation of the LDV data for the high loading case is given in McCormick et al.[4,5] and is summarized here. The downstream extent of the reversed flow was observed to increase to $3.3t$. Substantially more turning by the pressure side flow into the wake (compared to the low loading case) occurred. This increase in flow turning is attributed to the relatively weaker suction surface boundary layer, which induces greater pressure side flow turning by entrainment.

The separated flow region on the suction surface (high loading), as discussed previously, was intermittent in nature. This unsteadiness lead to a significant individual realization bias in the LDV data in this region. The bias occurred since a disproportionate number of realizations were from the high seed density "bursts" of downstream flow compared to the low seed density of the reversed flow.

The streamline pattern calculated from the LDV data is shown in Fig. 11 for the low loading case. It is the simplest method of categorizing the wake structure; however, as pointed out by Paterson,[2] the transverse flow in the wake centerline resides at the local mean value only a small fraction of the time due to the presence of vortex shedding. Thus caution should be exercised when interpreting the mean patterns. The $\psi = 0$ streamline (body value), which originates from the pressure side of the trailing edge, represents the "dividing streamline," which separates the time mean flow of the pressure surface from the flow of the suction surface. A second $\psi = 0$ streamline originates on the suction side and terminates on the trailing edge circle and thus forms a closed recirculation bubble attached to the trailing edge. Disagreement between the origins of the $\psi = 0$ streamlines and the separation locations shown in Fig. 11 is due to lack of high resolution LDV data near the trailing-edge surface. A more negative stream function value, say -0.02, defines a closed recirculation region located downstream of the trailing edge and a suction surface streamline that extends from negative to plus infinity. A streamline having an intermediate value of -0.013 extends from negative infinity on the suction side, turns upstream between the $\psi = 0$ and $\psi = -0.02$ recirculations and then turns downstream. Thus, in the mean, the flow from the suction side flows upstream to the pressure side of the trailing edge.

To explore this unusual streamline pattern, first consider the steady, symmetric case. Here, two $\psi = 0$ streamlines lift off the surface at the boundary-layer separation locations, enclose two symmetrical recirculation regions, and join downstream at a closure point. From the closure point, two $\psi = 0$ streamlines emerge, one that extends to downstream infinity and another that extends upstream and stagnates at the trailing edge. For this situation the two recirculations are closed and attached to the trailing edge, with no flow from the pressure and suction sides entering the region.

One interpretation of the flow pattern in Fig. 11 is that the strong pressure surface shear layer sets up a correspondingly strong clockwise recirculation region ($\psi = -0.02$), which entrains near stagnant suction side fluid. This could cause the $\psi = -0.013$ streamline to reverse and then proceed downstream between the dividing streamline and the $\psi = -0.02$ bubble.

It is noted that this streamline pattern bears a remarkable resemblance to the trailing-edge flow field predicted by Smith[11] for laminar, steady separations from sharp trailing edge air foil geometries. Smith's "moderate asymmetry" case showed one attached (suction side) and one off-body recirculation (pressure side) with suction surface flow moving upstream before turning downstream and passing over the top of the off-body recirculation. A recent Navier-Stokes analysis by Davis et al.[12] of the CDA cascade geometry has also displayed this flow pattern for a negative incidence angle with suction surface separation. Close inspection of the trailing edge region reveals that the suction surface recirculation is attached,

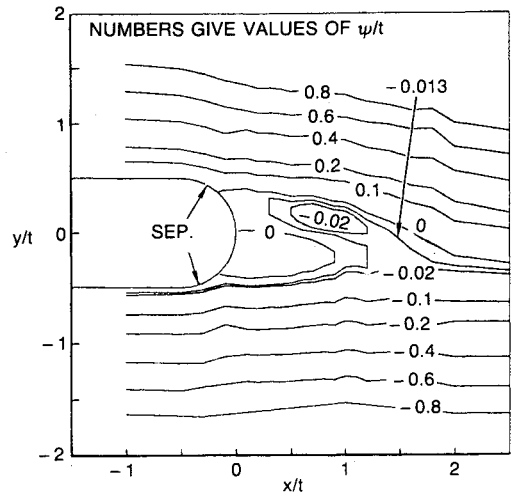

Fig. 11 Streamline pattern in near wake, low loading.

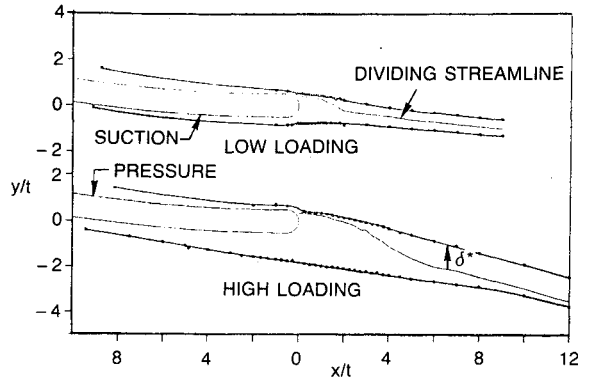

Fig. 12 Displacement thickness relative to trailing edge and dividing streamline.

bounded by the body stream function value and the pressure side recirculation is off-body, entraining suction side fluid.

The displacement and momentum thickness (δ^* and θ, respectively) were calculated from the LDV and hot film data upstream and downstream of the trailing edge using standard incompressible flow definitions. Upstream of the trailing edge, the integration was from the surface to the freestream. Downstream of the trailing edge, integration was from the dividing streamline to the local freestream. The normalizing velocity for the integration was the local freestream value and the integration line was normal to the trailing-edge metal angle.

At the top of Fig. 12 the displacement thickness distribution around the model and downstream of the trailing edge is shown for the low loading case. Upstream of the trailing edge, the displacement thickness decreases along the pressure surface and increases along the suction surface. This difference is due to the opposite pressure gradients acting on the respective boundary layers. Downstream of the trailing edge, the displacement surfaces converge for 3 trailing-edge thicknesses before becoming nearly parallel with a $0.7t$-$0.8t$ separation. Convergence is due to flow filling the wake. The dividing streamline is observed to undergo a rapid change between the two displacement surfaces over the first two trailing-edge thicknesses. Initially, the streamline is close to the pressure side displacement surface, then it deviates toward the suction side displacement surface before becoming essentially parallel with the pressure side. The rapid change in this streamline is believed to be due to pressure side flow, at the expense of its own momentum, energizing the suction side. That is, by turbulent and vortex mixing, slower fluid elements on the suction side are exchanged with faster elements on the pressure side. Thus in order to maintain the same mass flow between the displacement surfaces and the dividing streamline, the dividing streamline must migrate towards the suction side.

The high loading case, shown at the bottom of Fig. 12, illustrates the dramatic growth of the suction surface separated boundary layer. The suction surface displacement thickness at the trailing edge is more than 120% of the trailing-edge thickness (compared to 34% for the low loading case). The pressure surface displacement thickness is very similar to the low loading case. Downstream of the trailing edge, the displacement surfaces began to converge at a rate much slower than for low loading. The displacement surfaces are still converging at the end of the measurement domain and approaching an asymptotic value around $1.3t$ (nearly double that of the low loading case). The dividing streamline, similar to the low loading case, migrates significantly from the pressure side to the suction side but over a longer axial distance (roughly $3t$ for low loading and $6t$ for high loading).

For low loading, the effective airfoil shape is a mildly tapered extension of the airfoil similar to CDA wake of Hobbs.[1] The displacement surfaces deviate from the metal angle as the flow migrates to the cascade-exit angle. The dividing streamline deviates from the metal angle by 6 deg. For high loading, the effective airfoil shape is dramatically different. The displacement region is much larger and in this case, the asymptotic direction of the dividing streamline deviates from the metal angle by 15 deg. The effect of the upstream suction surface separation on the relative flow turning is evident in the figure. The suction surface separation causes an additional 9 deg of flow deviation (using the dividing streamlines as an estimate of the cascade-exit angle).

The momentum thickness distribution for the low loading case is shown at the top of Fig. 13 in terms of normalized momentum thickness potted vs normalized axial distance. Hot film data are displayed as squares. The pressure surface momentum thickness is seen to decrease toward the trailing edge as the suction surface momentum thickness increases. This behavior is related to the pressure gradient history (in the same manner as displacement thickness). Downstream of the trailing edge, the total momentum thickness (suction plus pressure side) shows a rapid increase for 2–3 trailing-edge thicknesses to a value $\theta/t = 0.52$. This region also corresponds to the area of rapid downward displacement of the dividing streamline. This displacement reflects energization of the suction side flow by the pressure side, and, from the momentum thickness data, it can be inferred that significant total pressure loss (mixing loss) occurs during this process.

The high loading momentum thickness data, given at the bottom of Fig. 13, shows similar trends as the low loading case. The pressure surface distribution is observed to be nearly the same as the low loading case (as was the displacement thickness). The suction side momentum thickness grows to

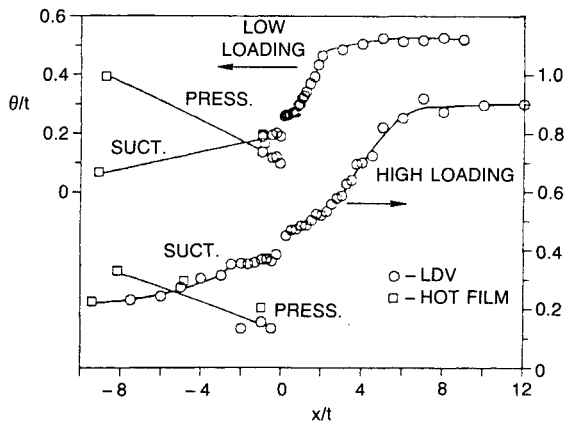

Fig. 13 Momentum thickness distribution.

twice the value of the low loading. Downstream of the trailing edge, the momentum thickness increases rapidly for 6–7 trailing-edge thicknesses to a value $\theta/t = 0.9$ (75% greater than for low loading). This region of increasing momentum thickness, as in the low loading case, is coincident with the region of dividing streamline migration.

Conclusions

The overall problem addressed in the current study was flow separation in the trailing-edge region of compressor airfoils. The specific focus of the study was to delineate the effects of pressure loading, thereby providing physical insight as well as experimental data of use to code development efforts. The study showed that loading effects were significant and need to be considered in the numerical modeling of the trailing-edge separated flowfield.

The primary effect of loading is concluded to be its influence, through different pressure and suction surface pressure gradient histories, on the strengths of the boundary layers approaching the trailing edge and the strengths of the resultant shear layers emanating from the separation locations. For the low loading case, the shape factors upstream of the trailing edge were 1.31 and 1.77 for the pressure and suction surfaces, respectively. This shape factor difference was not sufficient to alter separation locations on the trailing edge and base pressure from the unloaded case. However, this difference was sufficient to cause increased pressure side shear layer turning into the wake (by entrainment). This results in increased flow deviation from the trailing-edge metal angle and thus reduces airfoil circulation.

For the high loading case, the suction surface separation location was altered by the weak boundary layer strength, resulting in intermittent suction surface separation and base pressure depression. The large difference in the shape factors (1.24 on the pressure surface and 3.24 on the suction surface) caused much greater pressure side flow turning into the wake. Together with the streamline displacement created by the suction surface separation, this dramatically increased the flow deviation from the metal angle.

Based on these findings, incremental increases in airfoil turning from the low loading case to the high loading case will probably result in a gradual increase in flow deviation from the trailing-edge metal angle. This increasing deviation is primarily due to an increasingly larger shape factor difference between the suction and pressure surface boundary layers.

Acknowledgments

The study reported here was performed for Naval Air Systems command under contract N00014-83-C-0434. The authors wish to acknowledge Raymond P. Shreeve (Naval Postgraduate School), Michael J. Werle (UTRC), and Joseph M. Verdon (UTRC) for their helpful contributions in the formulation of this research program. Appreciation is also expressed to David E. Hobbs (Pratt & Whitney), Edward M. Greitzer (Massachusetts Institute of Technology), and Walter M. Presz Jr. (Western New England College) for helpful discussions during the course of the investigation. The assistance of William P. Patrick (UTRC) in placing a two-component laser velocimetry system into operation and Stanley A. Skebe's wind tunnel design contributions are also gratefully acknowledged. Also, the authors wish to acknowledge Charles C. Coffin and Keith A. Post for their assistance in conducting the experiment.

References

[1]Hobbs, D. E., Wagner, J. H., Dannenhoffer, J. F., and Dring, R. P., "Experimental Investigation of Compressor Cascade Wakes," American Society of Mechanical Engineers, New York, Paper 82-GT-299, April 1982.

[2]Paterson, R. W., and Weingold, H. D., "Experimental Investigation of a Simulated Compressor Airfoil Trailing-Edge Flowfield," *AIAA Journal,* Vol. 21, No. 5, 1985, pp. 768–775.

[3]Hobbs, D. E., and Weingold, H. D., "Development of Controlled Diffusion Airfoils for Multistage Compressor Application," *Journal of Engineering for Gas Turbines and Power,* Vol. 106, April 1984, pp. 271–278.

[4]McCormick, D. C., Paterson, R. W., and Weingold, H. D., "Experimental Investigation of Loading Effects on Simulated Compressor Airfoil Trailing-Edge Flowfields," United Technologies Research Center, East Hartford, CT, UTRC Rept. 87-14, Final Rept. for NASC Contract N00014-83-C-0434, May 1987.

[5]McCormick, D. C., Paterson, R. W., and Weingold, H. D., "Experimental Investigation of Loading Effects on Simulated Compressor Airfoil Trailing-Edge Flowfields," AIAA Paper 88-0365, Jan. 1988.

[6]Peacock, R. E., "Boundary-Layer Suction to Eliminate Corner Separation in Cascade Airfoils," Aeronautical Research Council, London, R&M No. 3663, 1971.

[7]Hama, F. R., "An Efficient Tripping Device," *Journal of the Aeronautical Sciences,* Vol. 24, March 1957, pp. 236–237.

[8]Roshko, A., "On the Drag and Shedding Frequency of Two-Dimensional Bluff Bodies," NACA TN-3169, July 1954.

[9]Deutsch, S., and Zierke, W. C., "The Measurement of Boundary Layer on a Compressor Blade in Cascade—Part 2: Suction Surface Boundary Layers," American Society of Mechanical Engineers, New York, Paper 87-GT-249, May–June 1987.

[10]Patrick, W. P, "Flowfield Measurements in a Separated and Reattached Flat Plate Turbulent Boundary Layer," NASA Contractor Rept. 4052, March 1987.

[11]Smith, F. T., "Interacting Flow Theory and Trailing Edge Separation—No Stall," *Journal of Fluid Mechanics,* Vol. 131, June 1983, pp. 219–249.

[12]Davis, R. L., Hobbs, D. E., and Weingold, H. D., "Prediction of Compressor Cascade Performance Using a Navier-Stokes Technique," *Journal of Turbomachinery,* Vol. 110, Oct. 1988, pp. 520–531.